Streamers in the JIPP T-IIU Tokamak Plasmas

Y. Hamada,* T. Watari, A. Nishizawa, K. Narihara, Y. Kawasumi, T. Ido, M. Kojima, K. Toi, and JIPPT-IIU Group

National Institute for Fusion Science, Toki 509-5292, Japan

(Received 15 June 2005; published 22 March 2006)

It is shown that the low-density Ohmically heated tokamak plasmas have streamerlike eddies at the outer region at normalized minor radius of about 0.7 and high-frequency zonal flows of large amplitudes in the core. The amplitudes of the eddies $e\tilde{\Phi}/kT_e$ and $\tilde{n}_e/\bar{n}_e$ are of order of 0.5, similar to that of blobs in the tokamak plasma boundary. The waveforms are featured by pulses of complex shape with sharp fronts, similar to the results of streamer simulations by Garbet *et al.*. The time constant of the fronts is also in agreement with the simulation. The radial span of the eddies is estimated to be much larger than the poloidal span.

DOI: 10.1103/PhysRevLett.96.115003 PACS numbers: 52.35.Ra

The regulation or suppression of plasma turbulence by sheared poloidal flow is regarded as one of the key issues of plasma confinement [1,2]. It is theoretically and numerically pointed out that the sheared poloidal flow can be generated by the nonlinear interaction of plasma turbulence itself and regulates the turbulence [3–11]. There are two extremely different types in the sheared poloidal flow, zonal flow and radially elongated eddy (streamer). The sheared zonal flow is characterized by small poloidal wave number ($k_p \approx 0$) and large radial wave number (k_r), while the streamer is characterized by small radial and large poloidal wave number. Streamers can cause large plasma transport, while the zonal flow will reduce the turbulent transport.

The streamer, as well as zonal flow in the toroidal device, is therefore a very challenging subject for the controlled fusion research since it is expected to have a large effect on the confinement of the high temperature plasma. Several experiments on low-frequency and high-frequency zonal flows have been reported using various diagnostics [12–19]. There is, however, only one experimental paper of the streamer up to now, in spite of its importance in the understanding of plasma confinement in toroidal devices [20]. One of the most powerful diagnostics for the study of these phenomena may be a heavy ion beam probe (HIBP) since it is possible to determine small-scale plasma flows (eddies) with slow velocity of order of diamagnetic drift velocity, through fast, local, and multipoint measurement of plasma potential (Φ) and basic plasma motion of E/B ($= -\nabla\Phi/B$), using HIBP [12,16–18].

Recently, correlation analysis of potential and density fluctuations measured by HIBP was conducted in the wide region of the plasma cross section of JIPP T-IIU tokamak plasmas [18]. It showed that the potential fluctuations of the core plasma inside the region of $r/a_p = 0.5$ are dominated by the $m = 0$ large oscillations in the geodesic acoustic mode (GAM) frequency range [21], with radial correlation length of 1–2 cm. In this Letter, we present the first experimental evidence of the streamer phenomena in the hot tokamak plasma at about normalized minor radius of 0.7, about 7 cm inside the LCFS (last closed flux surface) as possible origins of blob phenomena and try to show how the regions of zonal flow and streamers are separated in the tokamak cross section.

The experiment was carried out in JIPP T-IIU tokamak plasma with a nearly circular cross section and with the major and minor radii of 93 and 23 cm, respectively [22]. The main diagnostics are a Thomson scattering of YAG (yttrium-aluminum-garnet) laser light with 28 spatial measurement points and 100 Hz repetition rate to obtain detailed profiles of plasma density and electron temperature, an 8-channel electron cyclotron emission (ECE) polychromator, a 6-channel FIR interferometer, and a charge recombination spectrometer using neutral beam injection (NBI) to obtain ion temperature profiles.

The HIBP for the JIPP T-IIU tokamak facilitates the injection of a 50–500 keV thallium (Tl^+) beam of a few tens of microamps, and the detection of the secondary thallium beam (Tl^{2+}) ionized in the plasma [12,18,23]. The change of the energy of the Tl^{2+} beam and its intensity correspond to the local plasma potential and plasma density, respectively, where the ionization takes place (sample volume). The position, size, and the direction of alignment of 6 sample volumes (SVs) used in this experiment are shown in Fig. 1(a). They are specified by three parameters, i.e., primary beam energy ($j = A$, B, and C, for 450, 300, and 250 keV, respectively, under toroidal magnetic field of 3 T), poloidal injection angle ($k = 1$–6), and input slit number of an energy analyzer ($l = 1$–6). The beam energy is fixed during one plasma discharge. The injection angle is swept in steplike operation, stays for 5 ms at one angle and stays at different angle for another 5 ms, and so on. It is sometimes swept continuously by applying sawtoothlike voltage on the sweeper. A partial line designated by a combination of these 2 labels like A2, shall be called a "step" in this Letter. Figures 1(b) and 1(c) show an expanded view of how SVs look like at step A4 and step C2, respectively. The SVs are cylinders of about 2–4 mm in diameter, cut in slant angle with a side view of parallelogram. The length (longer diagonal of the parallelogram) is about 5 to 15 mm along the beam trajectory, depending on the three parameters. The frequency bandwidth of the

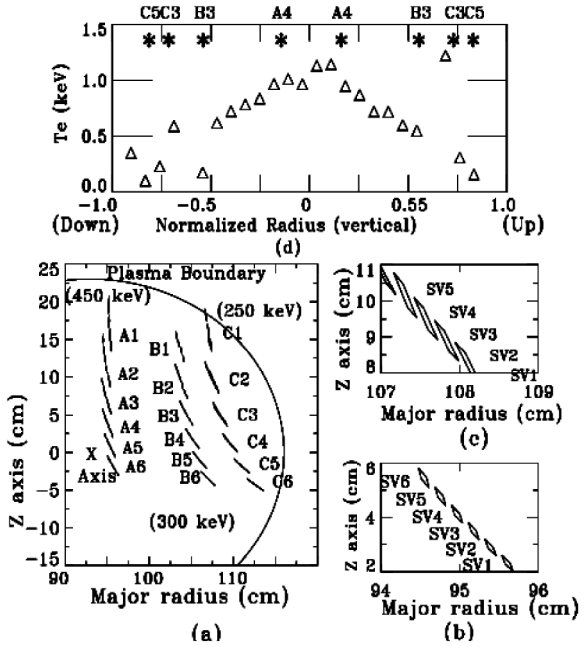

FIG. 1. (a) Location and direction of alignment of 6 SVs of the HIBP at 18 steps discussed in this Letter. Label A stands for the beam energy of 450 keV, label B for 300 keV, and label C for 250 keV. (b) Shape and positions for SVs at step A4 and (c) is for C2. (d) The vertical profile of electron temperature across the axis obtained by YAG Thomson scattering measurement. The positions of SVs at various steps are shown for reference.

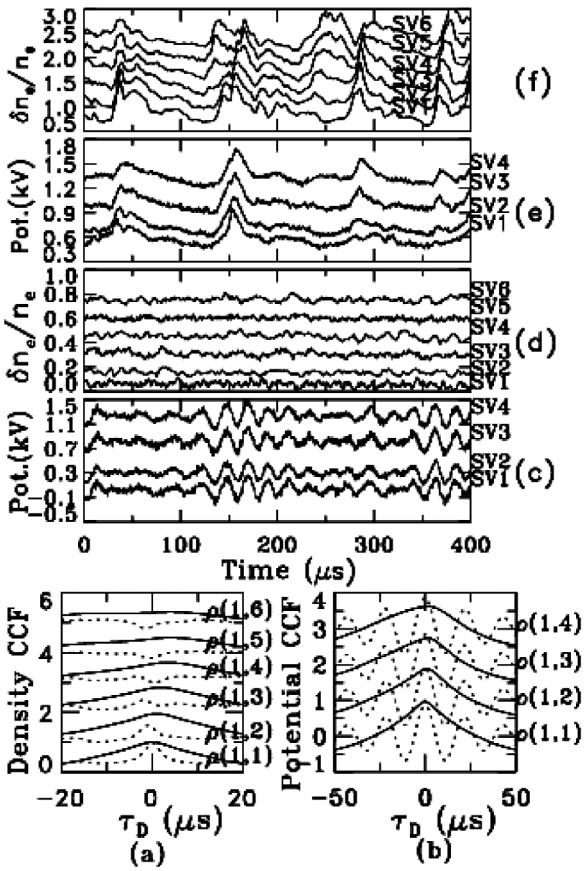

FIG. 2. (a) Correlation coefficient function (CCF) of density fluctuations at C2 and A4 (dotted line). (b) CCF of potential fluctuations at C2 and A4 (dotted curves). (c),(d) Time-expanded raw data of potential (c) and local density fluctuations (d) at A4. (e),(f) Raw data for potential (e) and density fluctuations (f) at C2. Correlation was taken between signals at SV1 and SV$_j$ [j = 1–6 for density (c) and j = 1–4 for potential measurement]. CCF for functions u and v, $\rho(u, v, \tau_d)$, is defined by $\rho(u, v, \tau_d) = C(u, v, \tau_d)/\sqrt{C(u, u, 0)}/\sqrt{C(v, v, 0)}$, where $C(u_i, v_j, \tau_d) = \int_{-T}^{+T} u_i(t)v_j(t + \tau_d)dt$. T is chosen as 2 ms in this analysis. Multiple curves are displaced upwards to avoid the overwriting. CCFs are displayed by shifting upwards by j^{-1}.

detector circuit at 3 dB gain decrease is 300 kHz limited by high-gain electric amplifiers used for the measurement of the secondary beam. The experiments were carried out under the following conditions [18]: The plasma current is 200 kA with a safety factor q value around 4.3 and a toroidal field of 3 T.

The average plasma density is low and is about 1×10^{13} cm^{-3} in order to allow good penetration of the beam to the core of the plasma. The vertical profile of electron temperature across the magnetic axis measured by 28-channel Thomson scattering apparatus is shown in Fig. 1(d). As shown in Fig. 1(d), the plasma is heated up to 1.1 keV in the core only by Ohmic heating. Ion temperature may be estimated to be less than 1/3 or 1/4, because electrons are heated only by Ohmic heating in these experiments and the energy transfer from the electron to ions is small because of low plasma density.

Figure 2 shows the difference of the correlation coefficient functions and time-expanded view of fluctuations at the core region of A4 and the outer region of C2. There is a sharp contrast in the characteristics of fluctuations at A4 and C2. The distinct pulses with large relative amplitude of density and potential, with sharp fronts, can be observed at step C2 [Figs. 2(e) and 2(f)], while large potential oscillations and very small density fluctuations [Figs. 2(c) and 2(d)] are observed at A4.

Another large difference is that the density fluctuations at the core region of A4 propagate in the direction of electron diamagnetic drift, and at C2–C6 regions density and potential fluctuations propagate at ion diamagnetic drift [Figs. 2(a) and 2(b)]. The dominance of the fluctuations propagating in the ion diamagnetic drift direction was observed as the ''edge ion mode'' by beam emission spectroscopy (BES) measurement at normalized minor radius of about 0.9 of L-mode plasmas of Tokamak Fusion Test Reactor [24]. In our case the dominance of the edge ion mode occurs at the normalized radius of about 0.7 in Ohmically heated plasmas and its region tends to shrink in NBI or ion cyclotron range of frequency heated plasmas [23].

Figures 3(b) and 3(c) show another typical example of the density and potential time behaviors at C5, where the SVs are mainly positioned radially. The density waveforms of Fig. 3(c) are complex and not solitary and have sharp ''fronts'' [8] or ''strong gradients'' [9,10], similar to those obtained in the streamer simulations of simplified MHD equations done by Garbet [8], Beyer *et al.* [9], and Benkadda *et al.* [10]. The predicted time constant of the fronts, 10–100 μs, is in agreement with our observation, order of 10 μs [8]. This value is about 100–1000 times shorter than that of the previously reported streamer measured by ECE [20].

The density and potential fluctuations tend to differ from each other in shape. The relative amplitudes, $e\tilde{\Phi}/kT_e$ and $\tilde{n}_e/\bar{n}_e$, are of order 0.5 as is in C2.

Figure 3(a) shows time behavior of the intensity of the secondary beam at detector plates (I_s), when SVs are swept continuously (not in step) at the 250 keV case by applying sawtooth voltage on the poloidal sweeper. The intensity grows at near C1 as the SVs enter into plasma boundary where the plasma density grows rapidly. Around C2 it tends to grow slowly and begins to decrease because the density slowly increases and the attenuation of the primary beam by electron ionization begins to dominate. The relative change of local plasma density ($\tilde{n}_e/\bar{n}_e$) can be observed as $\tilde{I}_s/\bar{I}_s$, and we can observe very frequent sharp pulses throughout the sweep of boundary-C1–C6-boundary. The relative amplitude is very high around C2 to C5.

Figure 4 shows that the difference of potentials between SV1 and SV2 and between SV3 and SV4, corresponding to the poloidal electric fields (E_θ) because SVs are positioned nearly at the same magnetic surface at C2, and the behavior of average density of SV1 and SV2 and that of SV3 and SV4. The pulsed E_θ of both curves of Fig. 4(a) is in most cases negative when the density increases significantly. The negative E_θ is for driving density out of the magnetic surface by E/B drift. The different behaviors of the upper and lower traces of Fig. 4(a), the fact that E_θ poloidal electric field changes its phase significantly, almost 90°, or 180° and sometimes at same phase, means that the radial flow velocity of the eddy changes its phase within the distance of twice the distance between SV1 and SV2, about 1 cm. Accordingly the poloidal span of these eddies may be order of 1 cm. The maximum E_θ of Fig. 4(a) is about 100 V/0.65 cm = 15 kV/m. Then the radial velocity at the eddies may be $E/B = 5$ km/s. The typical pulse length of 20 μs of Fig. 4(a) means the radial span of the eddies is order of 10 cm, similar to the depth of the layer of these eddies.

We can also estimate the radial span by $\tilde{n}_e/\bar{n}_e$. This value may be the product of the radial span of the eddies and the inverse gradient length of averaged plasma density. The position of C2 is well inside the plasma boundary where the density gradient length is long, as is shown in Fig. 3(a). Thomson scattering can estimate the density gradient length to be about 10 cm. Then the radial size may be order of 5 cm, which is larger than the poloidal characteristic length of about 1 cm.

There is also large difference in the density waveforms of SV1 and SV6 of Fig. 3(c). In almost all cases of Fig. 3(c), the pulse height grows or decays from SV1 to SV6. The radial size of the streamer is larger than the distance between SV1 and SV6, 3 cm, or is about the order of the distance. An accurate estimate of the size of the eddies by density measurement is, however, difficult because of the small spatial coverage of our HIBP system.

Since the poloidal characteristic length of the eddies is about 1 cm and is much smaller than the radial span, we are

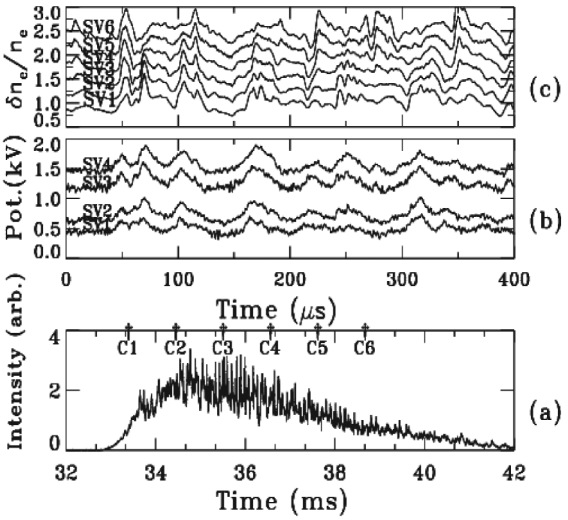

FIG. 3. (a) Time behavior of the intensity of the secondary beam, when the beam is swept continuously through C1–C6 instead of steps. (b),(c) Time-expanded view of raw data of density (b) and potential fluctuations (c) at C5.

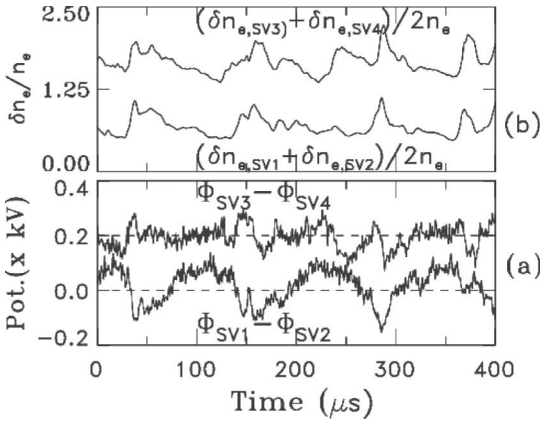

FIG. 4. (a) Difference of potentials $\Phi_{C,2,1} - \Phi_{C,2,2}$ (lower trace) and $\Phi_{C,2,3} - \Phi_{C,2,4}$ (upper trace) at C2. The dashed lines are zero lines. (b) $0.5[\tilde{n}_e/\bar{n}_e(\mathrm{SV}_{C,2,1}) + \tilde{n}_e/\bar{n}_e(\mathrm{SV}_{C,2,2})]$ (lower trace) and $0.5[\tilde{n}_e/\bar{n}_e(\mathrm{SV}_{C,2,3}) + \tilde{n}_e/\bar{n}_e(\mathrm{SV}_{C,2,4})]$ (upper trace). The upper curves are shifted upwards.

now able to ascribe our eddies at C2–C6 as streamers predicted by several papers [6–11]. Streamers are observed in C1–C6, B1, and A1, the outer region. At half-radius region of B2–B5, the amplitude of these streamers (sharp fronts) becomes smaller and appears only in density signals although the figure is omitted. In the core region of A3–A6, B3–B5, potential oscillations are dominated by GAM oscillations. The streamer phenomena are rare at steps A1 and B1, about 1 pulse/ms. In addition, the streamers occur much more often at C4 and C5, which are located near the equatorial plane, compared with C2. Since A1 and B1 have almost the same minor radii with C2, these facts mean that streamers have strong ballooning character.

The Fourier spectra of the density fluctuation measured at all steps are just governed by the broadband spectrum up to a few hundreds kHz, and there is no appreciable peak of GAM or so, in contrast to the potential fluctuations [18].

The waveforms of the pulses of a single peak at C2 shown in Fig. 2(e), as well as the relative amplitudes, are similar to that of IPO (intermittent plasma object) observed by the probe measurement placed near the LCFS in Dlll-D and other tokamaks [25–27], more widely known as blobs. The difference of IPO and streamers can be summarized in the following way: (1) The waveforms of the potential and density are different each other, while in IPO they are identical. (2) As shown in Figs. 3(b) and 3(c), the pulse is not solitary and often complex and very similar to the waveforms of the simulations [8–10], in contrast to solitary pulses of IPO. (3) The streamers in this Letter are observed where SVs are at 4–8 cm inside the LCFS and the electron temperature is about 400 eV. IPOs are observed at the LCFS and scrape-off layer. (4) The electron temperature measured by Thomson scattering shows large fluctuations around 400 eV in our case. In case of IPO the electron temperature shows large fluctuations at 150–100 eV [25].

As for the indication of streamers from other diagnostics, the ECE emission from plasma around C2–C5 is too weak to get a fast time response. The temperature profile obtained by YAG Thomson scattering always has irregularities around and outside B3, as shown in Fig. 1(d). The profile of the intensity of the scattered light is also disturbed similarly to Fig. 1(d), supporting that the large density fluctuations are present in this area. The detailed study of this effect will be studied in a full paper.

Throughout this Letter, $\tilde{n}_e/\bar{n}_e$ is calculated by the intensity of the secondary beam, neglecting change of temperature and path integral effect [23]. The effect of temperature variation on the ionization cross section of Tl is small if the temperature is above 100 eV. The density in these experiments is very low and the beam path is vertical and in right angle to the main direction of the streamer propagation, this effect is estimated to be very small.

In summary, the Ohmically heated plasmas, where the electron temperature is much higher than ion temperature, have a streamer region around the normalized radius of 0.7–1.0 and a region of high-frequency (GAM) zonal flow in the core. The streamer is often in the bad curvature region, i.e., ballooning characteristics. The region of half radius has sharp fronts with small amplitude only in the density perturbation. Potential perturbation is dominated by GAM oscillations. The streamer region (normalized radius of 0.7–1.0) coincides with the region, where the density turbulence propagates in the ion diamagnetic drift direction. The streamer has similar characteristics with the blobs, such as relative amplitude of order of 0.5 and time scale of 10 μs. The streamer has a feature of complex waveform, while that of the blob is simple because it is a circular object [25]. This finding may be brought by very small sample-volume of HIBP (2–3 mm in diameter and about 5 mm long as stated before) compared with that of other nonperturbing diagnostics like BES for local measurement in hot toroidal plasmas [14].

The authors would like to thank Professor K. Itoh for fruitful discussions.

*Also at Sokendai, Graduate University for Advance Study, Hayama 240-0163, Japan.

[1] H. Biglari and P. H. Diamond, Phys. Fluids B **2**, 1 (1990).
[2] K. H. Burrell, Phys. Plasmas **4**, 1499 (1997).
[3] A Hasegawa and M. Wakatani, Phys. Rev. Lett. **59**, 1581 (1987).
[4] Z. Lin *et al.*, Science **281**, 1835 (1998).
[5] B. Scot, Phys. Lett. A **320**, 53 (2003).
[6] P. H. Diamond *et al.*, Nucl. Fusion **41**, 1067 (2001).
[7] J. F. Drake, P. N. Guzdar, and A. B. Hassam, Phys. Rev. Lett. **61**, 2205 (1988).
[8] X. Garbet, Nucl. Fusion **39**, 2063 (1999).
[9] P. Beyer *et al.*, Phys. Rev. Lett. **85**, 4892 (2000).
[10] S. Benkadda *et al.*, Nucl. Fusion **41**, 995 (2001).
[11] W. Dorland *et al.*, Phys. Rev. Lett. **85**, 5579 (2000).
[12] Y. Hamada *et al.*, Fusion Eng. Des. **34–35**, 663 (1997).
[13] M. G. Shats and W. M. Solomon, Phys. Rev. Lett. **88**, 045001 (2002).
[14] G. R. McKee *et al.*, Plasma Phys. Controlled Fusion **45**, A477 (2003).
[15] G. S. Xu *et al.*, Phys. Rev. Lett. **91**, 125001 (2003).
[16] P. M. Schoch *et al.*, Rev. Sci. Instrum. **74**, 1846 (2003).
[17] A. Fujisawa *et al.*, Phys. Rev. Lett. **93**, 165002 (2004).
[18] Y. Hamada *et al.*, Nucl. Fusion **45**, 81 (2005).
[19] G. D. Conway *et al.*, Plasma Phys. Controlled Fusion **47**, 1165 (2005).
[20] P. A. Politzer, Phys. Rev. Lett. **84**, 1192 (2000).
[21] N. Winsor *et al.*, Phys. Fluids **11**, 2448 (1968).
[22] K. Toi *et al.*, in *Plasma Physics and Controlled Nuclear Fusion Research 1992* (IAEA, Vienna, 1993), Vol. 1, p. 519.
[23] Y. Hamada *et al.*, Nucl. Fusion **37**, 999 (1997).
[24] R. D. Durst *et al.*, Phys. Rev. Lett. **71**, 3135 (1993).
[25] J. A. Boedo *et al.*, Phys. Plasmas **8**, 4826 (2001).
[26] S. J. Zweben *et al.*, Phys. Plasmas **9**, 1981 (2002).
[27] J. A. Boedo *et al.*, Phys. Plasmas **10**, 1670 (2003).